



## A New Design of Dual Band Phase Shifter using MEMS Technology

B. A. Ganji \*, A. Razeghi

Department of Electrical and Computer Engineering, Babol University of Technology, Babol-484, IRAN

### PAPER INFO

#### Paper history:

Received 15 November 2012

Received in revised form 23 January 2013

Accepted 18 April 2013

#### Keywords:

MEMS

Dual Band

Phase Shifter

Coplanar Waveguide

Return And Insertion Losses

### ABSTRACT

This paper presents a new design of microwave microelectromechanical systems (MEMS) phase shifter for dual band wireless local area network (WLAN) applications. A bit is designed which produce a constant phase shift of  $11.25^\circ$  by switching between two lines that consist of 12 and 6 unitcells in each frequency band. A unitcell is constructed by gold membrane suspended over the coplanar waveguide (CPW) that can be moved vertically by electrostatic actuation. It can also ultimately be used for changing the operating frequency band. Two states of unitcell are used to switch between two frequency bands of 2.4 GHz and 5.2 GHz (IEEE 802.11 standard employed in dual band WLAN systems). First, a closed form equation of simplified model of the structure is obtained. Then, using this equation and advanced design system (ADS) simulator, the dual band phase shifter is designed. The validation of modeling and equations are demonstrated using the High Frequency Structure Simulator (HFSS). At the frequency of 2.4 GHz, maximum return and insertion losses are -16.96 and -0.12 dB, respectively that exhibit a phase shift efficiency of  $93.75\%$  ( $60.22\%$ ). At the frequency of 5.2 GHz, maximum return and insertion loss are -16.86 and -0.15 dB, respectively exhibiting a phase shift efficiency of  $75\%$  ( $60.22\%$ ). The new proposed design is only to achieve a dual band phase shifter using MEMS technology which has low loss and weight with high linearity respect to the other technologies.

doi: 10.5829/idosi.ije.2013.26.11b.09

## 1. INTRODUCTION

Nowadays, the development of communication system using the smart antenna increases the demand for the phase shifter with better performance and minimum size. In this case, the components that work in two frequency bands or more are very attractive because they reduce the size of multi-mode multi-band wireless communication systems. Microelectromechanical systems (MEMS) is chosen because of having low RF loss, low weight, high linearity and negligible DC power consumption in comparison with other technologies such as ferroelectric and MMIC (Monolithic Microwave Integrated Circuits) that are now implemented and have the advantage of high power handling and switching speed.

Only one RF MEMS phase shifter working on two frequencies has been presented using distributed MEMS transmission line (DMTL) design which does not have the capability of getting desired constant phase shift in two frequencies [1]. Constant phase shift in two frequencies, given in [2], was achieved by loaded line

design but it occupied very large space. In another work, the phase shifter could analogically achieve desired phase shift in two frequencies but the RF loss in upper frequency is undesired and the size of phase shifter is very large [3]. The phase shifter presented in [4] used GaAs technology the insertion gain of which was obtained with amplifier that limited the linearity of phase shifter. Using PIN diodes and switched line design and loading stubs in each line, constant phase shift in two frequencies was achieved in [5] but it seems that loading the stub caused an increase in the size of structure and RF loss.

In this paper, a new topology of phase shifter is presented that uses advantage of two designs of switched line and DMTL phase shifter which has the capability to work in multi band frequencies. 2.4 GHz and 5.2 GHz are chosen as design frequencies in terms of IEEE 802.11 standard that are employed in dual band WLAN systems. The switched line design produces true time delay (TTD) phase shifter and is easy to fabricate but in low frequencies it occupies large space. Distributed MEMS Transmission Line (DMTL) is employed instead of conventional transmission line which is used in switched line design and does not have

\*Corresponding Author Email: [baganji@nit.ac.ir](mailto:baganji@nit.ac.ir) (B. A. Ganji)

loading capacitance. This replacement helps us to reduce the size of phase shifter because of creating slow-wave structure. In addition, the phase shifter becomes capable of working in other operating frequencies by changing the propagation velocity of DMTL. Furthermore, we ensure in new design, the TTD feature remains in frequencies lower than Bragg frequency. The theoretical analysis of the structure is done and its performance is investigated using simulation in two frequency bands of [2.15-2.5] and [4.95-5.45] GHz. The simulation results show the feasibility of the new design with high phase shift efficiency.

**2. RF THEORETICAL ANALYSIS**

This new dual band phase shifter is a kind of switched lined phase shifter that each path of switch is constructed by DMTL to create desired phase in the operating frequency. A DMTL is constituted of some cascaded unitcell consisting of a MEMS bridge placed on the coplanar waveguide (CPW) (see Figure 1). DMTL generates two different phases, when the MEMS bridge is up and down. This can help us to change the operating frequency of the phase shifter to achieve a constant phase shift in two operating frequencies.

**2. 1. DMTL Design** The first step for designing of structure, a simplified model of DMTL has been employed and MEMS bridge as a shunt capacitor is considered with ignoring its resistance and inductive effect [6]. Moreover, the transmission line can also be modeled with capacitance and inductance per unit length without considering the loss in the first step of design (Figure 2). Using this model, the characteristic impedance of DMTL is given as [6]:

$$Z_{0l} = \sqrt{\frac{lL_t}{lC_t + C_b}} \sqrt{1 - \left(\frac{\omega}{\omega_B}\right)^2} \tag{1}$$

$$\omega_B = \frac{2}{\sqrt{lL_t(lC_t + C_b)}} \tag{2}$$

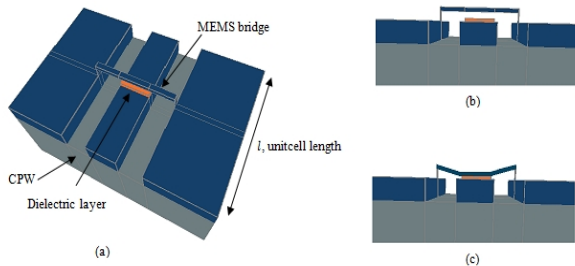


**Figure 1.** One unitcell of DMTL (a) 3D view of the unitcell (b) up state of the unitcell (c) down state of the unitcell

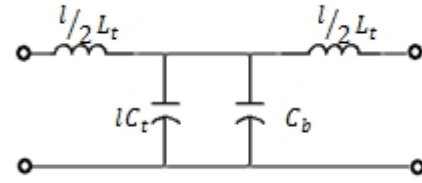


**Figure 2.** Simple model of a unitcell

where,  $\omega_B$  is the Bragg angular frequency,  $C_b$  is the capacitance of MEMS bridge,  $C_t$  and  $L_t$  are the capacitance and inductance per unit length of transmission line, respectively and  $l$  is the unitcell length that for accurate modeling must be very smaller than the wave length of transmission line in operating frequency. The transmission matrix of unitcell is equal with the unloaded transmission line, which has a different constant propagation from the transmission line of the unitcell, and then it's achieved:

$$1 + e^{2\gamma_{DMTL}} - (A + D)e^{\gamma_{DMTL}} = 0 \tag{3}$$

$$A = D = 1 - 2\left(\frac{\omega}{\omega_B}\right)^2 \tag{4}$$

where,  $\gamma_{DMTL}$  is the constant propagation equivalent of DMTL,  $A$  and  $D$  are the transmission matrix parameters of the unitcell. With solving above equations, the below result is obtained:

$$e^{\gamma_{DMTL}} = 1 - \frac{2\omega^2}{\omega_B^2} \pm j \frac{2\omega}{\omega_B} \sqrt{1 - \frac{\omega^2}{\omega_B^2}} \tag{5}$$

For  $\omega < \omega_B$  :

$$\gamma_{DMTL} = \alpha_{DMTL} + j\beta_{DMTL} = \frac{j}{l} \sin^{-1} \left( \frac{2\omega}{\omega_B} \sqrt{1 - \left(\frac{\omega}{\omega_B}\right)^2} \right) \tag{6}$$

The real part of  $\gamma_{DMTL}$  is referred to constant attenuation,  $\alpha_{DMTL}$ , that is zero and its imaginary part is called constant phase,  $\beta_{DMTL}$ , that shows the phase per unit length of the wave propagating. Note that changing  $C_b$ , which can be made by electrostatic actuation of the MEMS bridge, also leads to a change in DMTL constant phase and produces the phase shift. For  $\omega \ll \omega_B$  the phase shift is linear with frequency and produces constant delay with frequency that is called True Time Delay (TTD) feature. On the other hand, for  $\omega > \omega_B$ , there is only loss on DMTL and the waves cannot propagate. Thus, the operating frequency of DMTL is lower than Bragg frequency.

**2. 2. Transmission Line Theory** Now it is necessary to know, the capacitance,  $C_t$ , and inductance,  $L_t$ , per unit length of CPW transmission line. With

assuming the quasi-TEM propagation on the line, the below expressions are given [7]:

$$V_{ph} = \frac{C}{\sqrt{\epsilon_{eff}}} \tag{7}$$

$$Z_0 = \frac{1}{C_t V_{ph}} \tag{8}$$

$$L_t = C_t Z_0^2 \tag{9}$$

where,  $V_{ph}$  is the propagation velocity of wave on the line,  $C$  is the light velocity in free space,  $Z_0$  is the characteristic impedance of unloaded line of CPW and  $\epsilon_{eff}$  is the effective permittivity of CPW which is obtained by quasi static method of conformal mapping technique that is [7]:

$$\epsilon_{eff} = 1 + \frac{(\epsilon_r - 1) K(k_0) K(k_1')}{2 K(k_0') K(k_1)} \tag{10}$$

where,  $\epsilon_r$  is the relative permeability of substrate and  $K$  is the complete elliptic integral of first kind and the argument  $k_0$  and  $k_1$  are given by:

$$k_0 = \frac{c}{b} \sqrt{\frac{b^2 - a^2}{c^2 - a^2}} \tag{11}$$

$$k_1 = \frac{\sin\left(\frac{\pi c}{2h_{sub}}\right) \sqrt{\sin^2\left(\frac{\pi b}{2h_{sub}}\right) - \sin^2\left(\frac{\pi a}{2h_{sub}}\right)}}{\sin\left(\frac{\pi b}{2h_{sub}}\right) \sqrt{\sin^2\left(\frac{\pi c}{2h_{sub}}\right) - \sin^2\left(\frac{\pi a}{2h_{sub}}\right)}} \tag{12}$$

$$a = \frac{w}{2}, \quad b = \frac{w + 2g}{2}, \quad c = \frac{w + 2(g + s)}{2} \tag{13}$$

where,  $w$  is the center conductor width,  $g$  is the gap between the center conductor and sideways grounds,  $s$  is the ground width of CPW, and  $h_{sub}$  is the substrate height.  $k_0'$  and  $k_1'$  are the complementary modulus of  $k_0$  and  $k_1$ , respectively :

$$k_0' = \sqrt{1 - k_0^2}, \quad k_1' = \sqrt{1 - k_1^2} \tag{14}$$

**2. 3. Switched Line Design** The design uses the feature that the waves propagate on the transmission line has the phase which is proportional to the line length, then the phase shift can be achieved by switching the path propagation of the waves into another path with different length. The phase shift concept is obtained as:

$$\Delta\phi = \beta \Delta L \tag{15}$$

where,  $\beta$  and  $\Delta L$  are the constant phase of the transmission line and the difference length between two paths, respectively.

**2. 4. The Reconfigurable Dual Band Phase Shifter**

The main configuration of the dual band phase shifter is the switched line whose phase shift can be achieved by Equation (15). We need constant phase shift in two frequencies of  $f_{down}=2.4$  GHz and  $f_{up}=5.2$  GHz. In conventional switched line phase shifter, the phase shift of the line is proportional with frequency. In new proposed design for compensating the effect of frequency variation on the desired phase shift, the path of switched line is changed from conventional transmission line to DMTL for use of the capability of DMTL in producing phase shift with electrostatic actuation of the MEMS bridge.

Since there is only two operating frequencies, it is sufficient to consider two cases of DMTL for compensating phase shift with selecting the up and down modes of DMTL corresponding to MEMS bridge with applied zero voltage and actuation voltage, respectively. In order to compensate the reduction of phase shift which occurs with changing operating frequency from  $f_{up}$  to  $f_{down}$ , for lower frequency  $f_{down}$ , the down mode of DMTL is chosen in which,  $C_b$  is greater than the up mode of DMTL and which subsequently generates extra phase shift, as shown in Equations (2) and (6). The phase shift of the new proposed design can be achieved from Equation (15):

$$\Delta\phi = \begin{cases} \beta_{DMTL,down} \Delta L & , & f = f_{down} \\ \beta_{DMTL,up} \Delta L & , & f = f_{up} \end{cases} \tag{16}$$

where,  $\beta_{DMTL,up}$  and  $\beta_{DMTL,down}$  are the constant phase equivalents of DMTL which were achieved using Equations (2) and (6) by replacement of  $C_b$  with  $C_{up}$  and  $C_{down}$ , respectively. Therefore, the constant phase shift in both frequencies can be achieved by specifying the value of  $C_{up}$  and  $C_{down}$  correctly.

On the other hand, to have practical phase shifter, minimum insertion and reflection loss is needed. Thus, we need to specify the parameter of phase shifter through the optimization process. It's better first the closed form equation is obtained for RF losses of phase shifter. As mentioned above, DMTL can be substituted with the unloaded line that having the characteristic impedance and constant phase of  $Z_{o1}$  and  $\beta_{DMTL}$  respectively. Therefore, the scattering parameters can easily be obtained through reflection and transmission coefficient concept. Then, the return loss of one path of the new proposed phase shifter will be:

$$S_{11} = \Gamma_{in} = \Gamma_0 \frac{1 - e^{-j2\beta_{DMTL}L}}{1 - \Gamma_0^2 e^{-j2\beta_{DMTL}L}} \tag{17}$$

$$\Gamma_0 = \frac{Z_{o1} - Z_{00}}{Z_{o1} + Z_{00}} \tag{18}$$

where,  $\Gamma_{in}$  is the reflection coefficient at the input of the path consisting of consecutive reflections,  $\Gamma_0$  is the reflection coefficient at the input of the path without

considering consecutive reflections,  $L$  is the length of path and  $Z_{00}$  is the 50 ohm impedance that should be at the port of device for calculating the scattering parameters.

The insertion loss of the path is affected by the power reflected from input port and the power loss due to dielectric, conductor and radiative losses. Only conductor loss is considered, because the dielectric loss is very negligible compared with conductor loss. The radiative loss can also be neglected in the operating frequency by applying thin substrate compared to wave length of structure as below [8]:

$$h_{\text{sub}} \leq 0.1\lambda_{\text{cpw,up}} \quad , \quad \lambda_{\text{cpw,up}} = \frac{V_{\text{ph}}}{f_{\text{up}}} \quad (19)$$

where,  $\lambda_{\text{cpw,up}}$  is the wave length of CPW in upper frequency  $f_{\text{up}}$ . The above condition causes the radiation to start far above the upper operating frequency. The attenuation per unit length due to conductor loss,  $\alpha_c$ , that is specified through skin-effect loss analysis is given as [9]:

$$\alpha_c = \frac{R_s \sqrt{\epsilon_{\text{eff}}}}{480 \pi K(k_0) K'(k_0) (1 - k_{ab}^2)} \times \left\{ \begin{array}{l} \frac{1}{a} \left[ \pi + \log \left( \frac{4\pi(2a)}{t} \frac{1 - k_{ab}}{1 + k_{ab}} \frac{1 + k_{ac}}{1 - k_{ac}} \right) \right] \\ + \frac{1}{b} \left[ \pi + \log \left( \frac{4\pi(2b)}{t} \frac{1 - k_{ab}}{1 + k_{ab}} \frac{1 - k_{bc}}{1 + k_{bc}} \right) \right] \left( \frac{1 - k_{ac}^2}{1 - k_{bc}^2} \right) \\ + \frac{1}{c} \left[ \pi + \log \left( \frac{4\pi(2c)}{t} \frac{1 + k_{ab}}{1 - k_{ab}} \frac{1 - k_{bc}}{1 + k_{bc}} \right) \right] \left( \frac{1 - k_{ab}^2}{1 - k_{bc}^2} k_{bc}^2 \right) \end{array} \right\} \quad (20)$$

where,  $t$  is conductor thickness and  $k_{ab}$ ,  $k_{ac}$ ,  $k_{bc}$  are the various aspect ratios of CPW and are defined as:

$$k_{ab} = \frac{a}{b} \quad , \quad k_{ac} = \frac{a}{c} \quad , \quad k_{bc} = \frac{b}{c} \quad (21)$$

And  $R_s$  is the series resistance due to skin effect, is given by:

$$R_s = \sqrt{\frac{\pi f \mu_0 \mu_r}{\sigma}} \quad (22)$$

where,  $\sigma$  is the conductor conductivity,  $\mu_0$  is the permeability of free space and  $\mu_r$  is the relative permeability of conductor. Since the attenuation is proportional to time average of power loss to the twice of time average of power transmitted to device [10], the insertion loss of the path can be described using the definition of scattering parameters as below:

$$S_{21} = \sqrt{1 - |S_{11}|^2 - 2\alpha_c L} \quad (23)$$

### 3. MECHANICAL THEORETICAL ANALYSIS

A constant actuation voltage applied between center conductor and side grounds of CPW, creates electrostatic

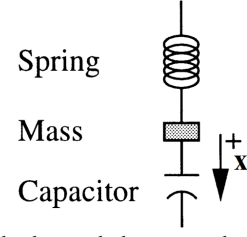


**Figure 3.** First order lumped electro-mechanical model of a MEMS bridge

force between them, and then pulls MEMS bridge toward the center conductor. A lumped electro-mechanical model consisting of a linear spring, a mass, and a parallel plate capacitor, as shown in Figure 3, can be considered for analysis of MEMS bridge behavior. The model assumes membrane's restoring force is a linear function of its displacement, neglects all electrical fringing fields and membrane curvature when considering the electrical forces on the membrane, takes all conductors and contacts to be perfect and then assumes that MEMS bridge operates in a vacuum, which is equivalent to neglecting any loading of the membrane. Conceptually, the equation of motion for MEMS bridge due to the electrostatic attraction force caused by a constant actuation voltage,  $V$ , can be expressed as [11]:

$$M \frac{d^2 x}{dt^2} - \frac{\epsilon_0 A V^2}{2(d_0 - x)^2} + kx = 0 \quad (24)$$

where,  $M$  is membrane mass and  $k$  represents the spring effect for an electrostatically actuated MEMS bridge.  $\epsilon_0$  is the free space permittivity,  $A$  is the area of the capacitor plates,  $x$  is displacement in the direction as shown in Figure 3 and  $d_0$  is the separation of the capacitor plates at rest. As constant actuation voltage,  $V$ , is increased, there is a point which the electrostatic force overcomes the spring's restoring force, and MEMS bridge collapses [11]:

$$k = \frac{27\epsilon_0 A V_{PI}^2}{8d_0^3} \quad , \quad x_{PI} = \frac{d_0}{3} \quad (25)$$

where,  $x_{PI}$  is the point that collapse happens,  $V_{PI}$  is the pull-in voltage. Since at the pull-in point, the electrostatic pressure is equal with the elastic restoring pressure, the functional load-deflection characteristic of a fixed-fixed beam under uniform pressure can be used to obtain pull-in voltage [12]:

$$P_{\text{mec}} = \left[ 9.35 \left( \frac{\sigma t_m}{(w + 2g)^2} \right) + 32.36 \left( \frac{E_v t_m^3}{(w + 2g)^4} \right) \right] x + 24.35 \left( \frac{E_v t_m}{(w + 2g)^4} \right) x^3 \quad (26)$$

$$\sigma = \sigma_o (1 - \nu) \tag{27}$$

$$E_v = \frac{E}{\left( 1 - \nu^2 \left( \frac{\left( \frac{W}{w + 2g} \right)}{0.03 + \left( \frac{W}{w + 2g} \right)} \right)^{1.77} \frac{W^{-0.061}}{t_m} \right)} \tag{28}$$

where,  $P_{mec}$  is the uniform pressure,  $E$  represents the Young's modulus,  $E_v$  is the effective Young's modulus for a wide beam ( $W > 5$ ). Whereas for fixed-fixed beams, the effective residual stress is expressed as  $\sigma$  where  $\sigma_o$  is the residual stress and  $\nu$  is the Poisson's ratio. The electrostatic pressure,  $P_{elec}$ , can be obtained by differentiating the potential energy of the capacitor respect to the mass position:

$$P_{elec} = \frac{d}{dx} \left( \frac{1}{2} \frac{CV^2}{A} \right) \tag{29}$$

The capacitor is obtained using equation of IC wire capacitance approximation formula [13]:

$$C = \epsilon_o W \left( \frac{W}{h_a - x + \frac{h_i}{\epsilon_{ri}} + \frac{1.06 t_m^{0.5}}{(h_a - x + h_i)^{0.5}}} + \frac{1.06 W^{0.25}}{(h_a - x + h_i)^{0.25}} + 0.77 \right) \tag{30}$$

where,  $\epsilon_{ri}$  is the relative permittivity of insulation layer,  $t_m$  is the thickness of membrane,  $h_a$  is the initial gap between bridge and insulation layer. In addition, to existence of air between bridge and center conductor in unitcell, there is a thin layer of silicon nitride with thickness of  $h_i$  also on center conductor to prevent ohmic contact and increasing aspect ratio of  $C_{down}$  to  $C_{up}$ . One dimension of capacitive area is center conductor width,  $w$ , and another one is  $W$ . The electrostatic pressure and the elastic restoring pressure can be solved simultaneously to yield the final closed-form expression for the pull-in voltage:

$$V_{PI} = \frac{0.1414}{(w + 2g)^2} \sqrt{E_v x_{PI} A t_m \left( 3236 t_m^2 + 2435 x_{PI}^2 \right) \left( \frac{\partial C}{\partial x} \right)_{x=x_{PI}}} \tag{31}$$

The Pull-in voltage and spring constant are important characteristics of MEMS bridge that effect on RF performance. With larger mechanical stiffness of the structure, the nonlinearity decreases [14]. The pull-in voltage is maximum constant voltage can be applied to vary the capacitance of MEMS bridge linearity. In this paper, the actuation voltage larger than pull-in voltage applied to use maximum capacitance of MEMS bridge in down mode.

#### 4. DESIGN OF THE DUAL BAND PHASE SHIFTER

The bit is constructed by two paths of 22.5° and 11.25° switched to create a phase shift of 11.25°. Because of longer path, 22.5°, is lossy due to the constitution of more number of unitcells, it is chosen for optimization process. The goal is:

$$\begin{cases} \varphi = 22.5^\circ \\ S_{11} < -15 \text{ dB} \\ S_{21} > -0.5 \text{ dB} \end{cases} \tag{32}$$

For

$$\begin{cases} f = f_{down} & \text{and} & C_b = C_{down} \\ f = f_{up} & \text{and} & C_b = C_{up} \end{cases} \tag{33}$$

Before optimization, it is necessary to be known that what kind of effects, the parameters have on the goals. With this knowledge, some of the parameters should not be considered in optimization process because they have no effects on the goals or their optimize value can initially be specified. Therefore, the speed of optimization process could be increased.

In fact,  $s$  is the limitation in width of side ground metallization in conventional CPW due to space consideration that has not more effect on characteristics of line [7]. Hence, any value for this parameter can be chosen. Using Equation (23), the effect of CPW conductor thickness,  $t$ , on insertion loss can be seen. Figure 4 shows this effect when the other parameters are constant. As shown in Figure 4 when CPW conductor thickness increases, the insertion loss decreases, so the maximum value of 5µm is chosen for CPW conductor thickness.

For the consideration of other parameters effects, this conception is used that the maximum phase shift for minimum loaded capacitance is needed for minimum return loss. Just for this reason, to work in two frequencies the maximum phase shift sensitivity to loaded capacitance variation is needed.

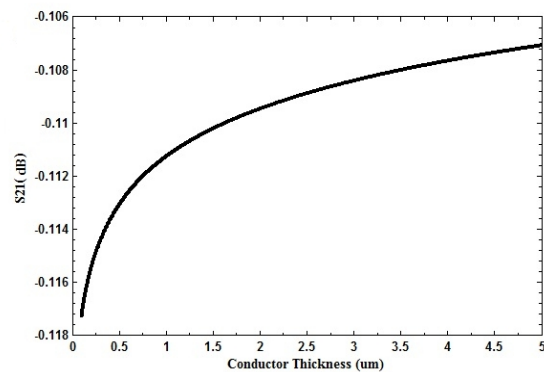


Figure 4. Insertion loss of DMTL vs. CPW conductor thickness when other parameters are constant



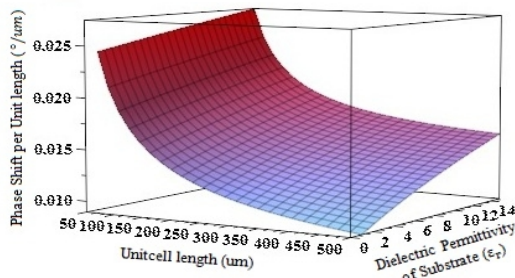
For this reason, the equations expressed in following are used:

$$\beta_{DMTL} = \frac{2\pi f}{V_{ph}} = 2\pi f \sqrt{L_t \left( C_t + \frac{C_b}{l} \right)} \quad (34)$$

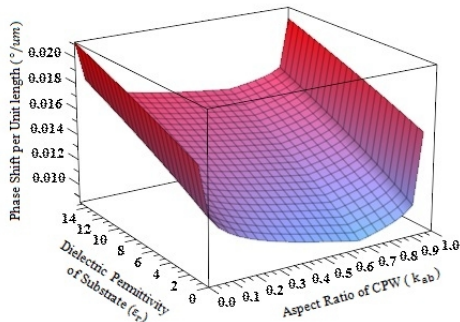
That is the approximate of Equation (6) in the operating frequency of  $\omega \ll \omega_B$ . This equation defines phase shift per unit length. Using it, phase shift sensitivity to loaded capacitance variation is obtained as below:

$$\frac{\partial \beta_{DMTL}}{\partial C_b} = \frac{\pi f}{l} \frac{L_t}{\sqrt{\left( C_t + \frac{C_b}{l} \right)}} \quad (35)$$

The effects of the parameters ( $l, k_{ab}, \epsilon_r$ ) on phase shift and its sensitivity are obtained using Equations (34) and (35) that shown in Figures 5 and 6, respectively. As other parameters are constant, decrease in value of  $\epsilon_r$ , increase phase shift sensitivity and decrease phase shift per unit length but since the former effect is much more than latter effect, a substrate with lower constant dielectric such as quartz ( $\epsilon_r=3.8$ ) with  $500\mu\text{m}$  thickness is chosen. The other design parameters such as  $w, g, C_{down}, C_{up}, l$  and  $L$  are specified by optimization process to satisfy Equation (32). The optimization process has been done by Agilent ADS, and the results has been shown in Table 1.

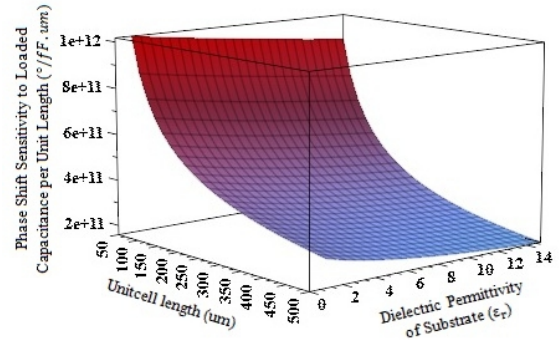


(a)

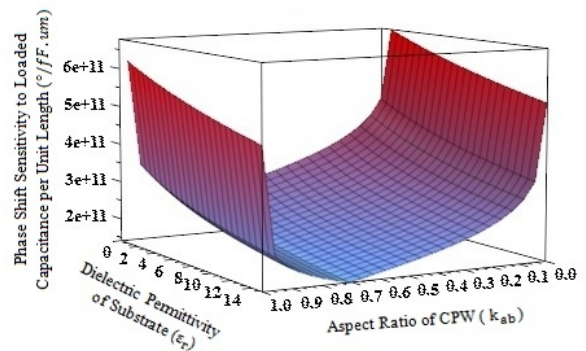


(b)

**Figure 5.** Phase shift per unit length depend on (a) the unitcell length and the dielectric permittivity of substrate (b) the aspect ratio of CPW,  $k_{ab}$ , and the dielectric permittivity of substrate for constant value of the unitcell length



(a)



(b)

**Figure 6.** Phase shift sensitivity to loaded capacitance per unit length depend on (a) the unitcell length and the dielectric permittivity of substrate (b) the aspect ratio,  $k_{ab}$ , and the dielectric permittivity of substrate

**TABLE 1.** Optimum parameters obtained using Agilent ADS simulation

L(mm)	l(μm)	w(μm)	g(μm)	C <sub>down</sub> (fF)	C <sub>up</sub> (fF)
1.868	155.64	133.45	109.98	50.64	3.58

**TABLE 2.** Design Parameters of MEMS bridge

Parameter	Value
membrane material	gold
membrane thickness, $t_m$	1 μm
membrane width, W	5 μm
Young's modulus, E	74.48 GPa
Poisson's ratio, $\nu$	0.42
membrane residual stress, $\sigma$	0 MPa
Air gap thickness, $h_a$	5.68 μm
insulator material	$\text{Si}_3\text{N}_4$
relative permittivity of insulator, $\epsilon_{ii}$	7.5
insulator thickness, $h_i$	0.95 μm

As mentioned above,  $C_{up}$ ,  $C_{down}$  are the MEMS bridge capacitance when zero and actuation voltage are applied between center conductor and side grounds of CPW, respectively. Till now, the values of  $C_{up}$ ,  $C_{down}$  and one dimension of capacitive area that is the center conductor width,  $w$ , have been specified. Other parameters related to MEMS bridge dimensions are obtained using Equation (30). Table 2 shows the design parameters of MEMS bridge.

## 5. RESULTS AND DISCUSSION

Now, all necessary parameters to design the new proposed phase shifter have been specified. As mentioned above, the phase shifter has been composed of two lines as reference line and main line that switches from reference line to main line to create desired phase shift. This paper aims to spot feasibility of the new proposed design for which ideal SPDT switch without loss and length is used. Ansoft HFSS is used that is a 3D full wave simulator solving Maxwell equations on the structures using the FEM method to obtain its scattering parameters. This result shows feasibility of the structure. In addition, the result of ADS simulation and theoretical analysis are employed to show how MEMS bridge modeling is true as a capacitance that used in design and the closed-form equation obtained by this modeling is valid. Furthermore, the capacitance of MEMS bridge versus the applied voltage is obtained using Intellisuite software with FEM method to analysis the electromechanical structure.

**5.1. The S-Parameters Characterization** Figure 7 shows the simulated return and insertion loss of the dual band phase shifter in lower frequency band where all MEMS bridges have been actuated. For working in upper frequency band, the applied voltage should be zero. Simulated return and insertion loss of the dual band phase shifter in upper frequency band have been shown in Figure 8. The return and insertion loss obtained through analytical and ADS and HFSS simulation have little difference in both lines. The difference between analytical and ADS simulation is due to approximation in obtaining the closed form equation of return loss such as neglecting the effect of conductor thickness and frequency in line characteristic and continuous reflection due to loading the line. Increase in frequency and conductor thickness decrease the characteristic impedance [7] which decreases the return loss in terms of Equation (17) in high impedance lines. In addition, the effect of continuous reflection is increase in return loss that can be neglected in DMTL with low number of unitcell and low frequencies.

Moreover, neglecting substrate loss in theoretical analysis can create differences between insertion loss

obtained using analytical and ADS simulation results. The difference between ADS and HFSS simulation results is due to simplified modeling of MEMS bridge as a capacitance and neglecting its inductivity effect and loss. At the lower design frequency of 2.4 GHz, maximum return and insertion loss are -16.96 and -0.12 dB, respectively that exhibit a loss of -0.12dB/bit and a phase shift efficiency of 93.75 °/dB and 60.22 °/cm. At the upper design frequency of 5.2 GHz, maximum return and insertion loss are -16.86 and -0.15 dB, respectively, that exhibit a loss of -0.15dB/bit and a phase shift efficiency of 75 °/dB and 60.22 °/cm.

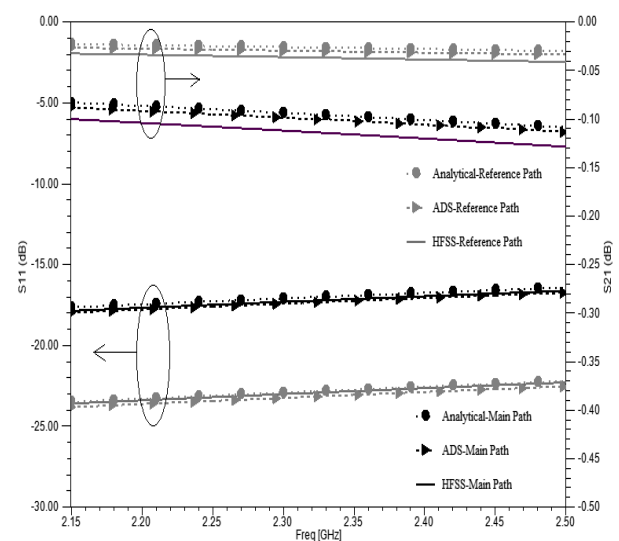


**Figure 7.** Return and insertion loss of the dual band phase shifter in lower frequency band which the all MEMS bridge have been actuated

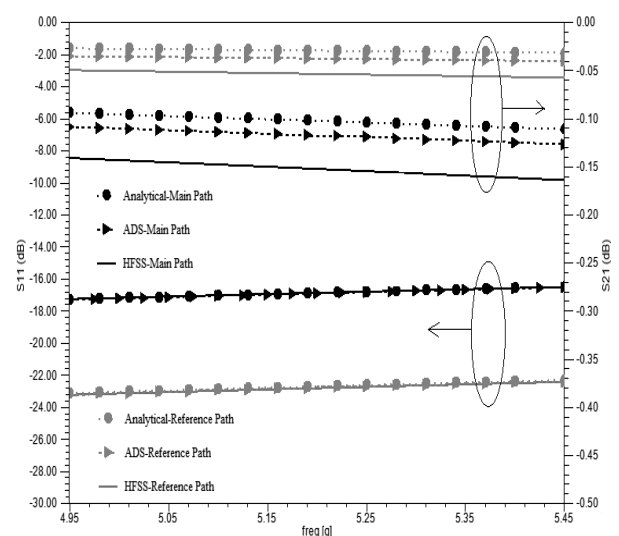


**Figure 8.** Return and insertion loss of the dual band phase shifter in upper frequency band which the all MEMS bridges have not been actuated

**5. 2. The Phase Shift** Figures 9 and 10 show the phase shift and its error in lower and upper frequency band, respectively. This error is obtained using differences between HFSS simulation result and design target that has a range of  $-0.77^\circ$  to  $0.89^\circ$  and  $-0.61^\circ$  to  $0.44^\circ$  in lower and upper frequency band, respectively. The differences are also seen between Analytical and ADS and HFSS results. This error is a less than  $0.89^\circ$  in whole of two bands and its reason have been explained in previous section. Figures 9 and 10 show the phase shift is linear with frequency and all results have the same and constant slope that is a time delay created by the phase shifter. In other words, the dual band phase shifter has the feature of true time delay (TTD) in each band.

**5. 3. MEMS Bridge Actuation** The phase shifter uses two states (up and down) of MEMS bridge creating two capacitances of  $C_{up}$  and  $C_{down}$  to change the operating frequency.

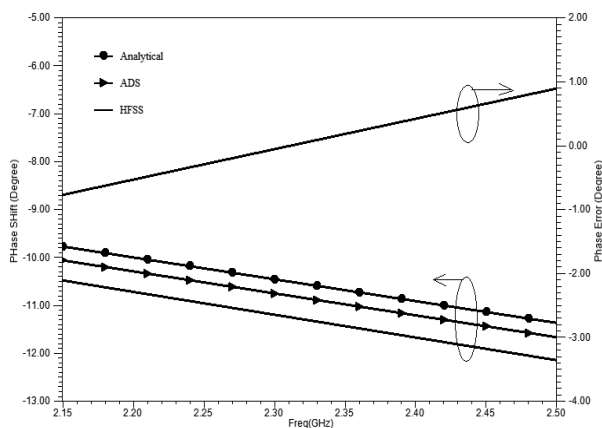


**Figure 9.** Phase Shift and Phase Error of the dual band phase shifter in lower frequency band which the all MEMS bridges have been actuated

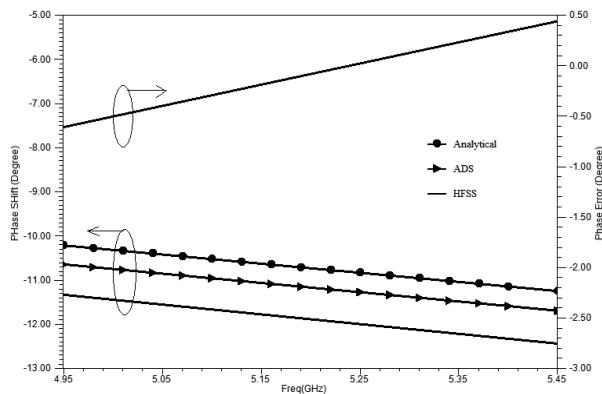


**Figure 10.** Phase Shift and Phase Error of the dual band phase shifter in upper frequency band which the all MEMS bridges have not been actuated

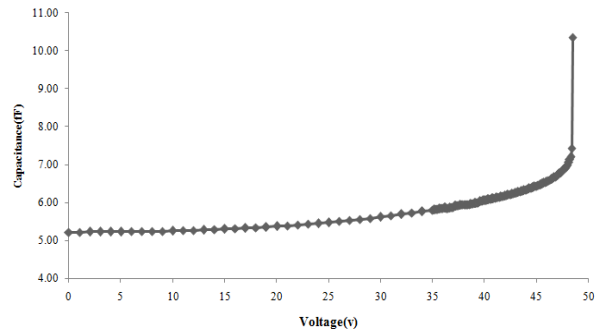


**Figure 11.** The simulation result of capacitance value of MEMS bridge versus applied voltage

**Displacement( $\mu\text{m}$ )**

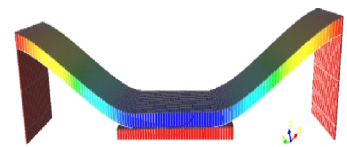
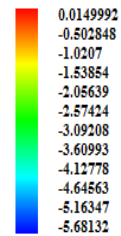


**Figure 12.** MEMS bridge when the actuation voltage is bigger than the pull-in voltage

As mentioned above, one capacitance is obtained with zero bias voltage and another one can be obtained when the bias voltage is bigger than the pull-in voltage. The capacitance value of MEMS bridge versus applied voltage was obtained using MEMS simulation tool (see Figure 11). It can be seen that, once the voltage value reaches 48.4 V, the capacitance value increases very much suddenly. Therefore, the simulated pull-in voltage is 48.4 V and calculated value using Equation (31) is 53.7 V. The difference between results is due to approximations to obtain the closed form equation of pull-in voltage. The down state of MEMS bridge is shown in Figure 12. Based on simulation, the actuation voltage of 51.8 V is applied to obtain the desired capacitance in down state.

**6. CONCLUSION**

A new design of microwave microelectromechanical systems (MEMS) phase shifter for dual band WLAN applications has been introduced. The phase shifter produces a constant phase shift which is created by switching between two lines with difference length in each frequency band. Each line has been constructed by cascade of unitcells. Two states of unitcells are used for switching between two frequency bands. Using the obtained closed form equation of simplified model of



structure and ADS simulator an 11/25° bit of the dual band phase shifter is designed. The HFSS simulation result shows the maximum return and insertion loss of -16.63 and -0.129 dB in lower frequency band of 2.15-2.5 GHz, respectively. It also shows the maximum return and insertion loss of -16.49 and -0.164 dB in upper frequency band of 4.95-5.45 GHz, respectively. A phase error relative to design is less than 0.89° in each frequency band. The new proposed dual band phase shifter exhibit a loss of -0.12 dB/bit and a phase shift efficiency of 93.75 %/dB and 60.22 %/cm in lower design frequency of 2.4 GHz, and a loss of 0.15 dB/bit and a phase shift efficiency of 75 %/dB and 60.22 %/cm in upper design frequency of 5.2 GHz. The simulation results show the feasibility of the new design with high phase shift efficiency.

## 7. REFERENCES

1. Tang, K., Wu, Y.-m., Wu, Q., Wang, H.-l., Zhu, H.-c., and Li, L.-W., "A novel dual-frequency rf mems phase shifter", in Electromagnetic Compatibility and 19th International Zurich Symposium on Electromagnetic Compatibility, APEMC Asia-Pacific Symposium on, IEEE. (2008), 750-753.
2. Tang, X. and Mouthaan, K., "Dual-band class iii loaded-line phase shifters", in Microwave Conference Proceedings (APMC), Asia-Pacific, IEEE. (2010), 1731-1734.
3. Ocera, A., Sbarra, E., Gatti, R. V. and Sorrentino, R., "An innovative reconfigurable reflection-type phase shifter for dual band wlan applications", in Microwave Conference, 36th European, IEEE. (2006), 64-67.
4. Banbury, D. R., Fayyaz, N., Safavi-Naeini, S. and Nikneshan, S., "A cmos 5.5/2.4 ghz dual-band smart-antenna transceiver with a novel rf dual-band phase shifter for wlan 802.11 a/b/g", in Radio Frequency Integrated Circuits (RFIC) Symposium, 2004. Digest of Papers, IEEE, (2004), 157-160.
5. De Luis, J. R. and de Flaviis, F., "A reconfigurable dual frequency switched beam antenna array and phase shifter using pin diodes", in Antennas and Propagation Society International Symposium, APSURSI'09. IEEE, (2009), 1-4.
6. Rebeiz, G., "Rf mems theory, design and technology, 2003", **Hoboken NJ: Wiley**,
7. Simons, R. N., Coplanar waveguide circuits, components, and systems, Wiley, (2001)
8. Aghamoradi, F., The development of high quality passive components for sub-millimetre wave applications., University of Glasgow, (2012)
9. Akgun, C. E., Drayton, R. F., Amey, D. I. and Mobley, T. P., "Application of uniplanar structures for high frequency material characterization", International Society for Optical Engineering, (2003), 621-626.
10. Cheng, D. K., "Field and wave electromagnetics", Addison-Wesley New York, Vol. 2, (1989).
11. Ladabaum, I., Jin, X., Soh, H. T., Atalar, A. and Khuri-Yakub, B., "Surface micromachined capacitive ultrasonic transducers", **Ultrasonics, Ferroelectrics and Frequency Control, IEEE Transactions on**, Vol. 45, No. 3, (1998), 678-690.
12. Chowdhury, S., Ahmadi, M. and Miller, W. C., "A new method of electrostatic force modeling for mems sensors and actuators", in MEMS, NANO and Smart Systems, International Conference on, IEEE., (2005), 431-435.
13. Somjit, N., Stemme, G. and Oberhammer, J., "Binary-coded 4.25-bit w-band monocrystalline-silicon mems multistage dielectric-block phase shifters", **IEEE Transactions on Microwave Theory and Techniques**, Vol. 57, No. 11, (2009), 2834.
14. Van Der Meijs, N. and Fokkema, J., "Vlsi circuit reconstruction from mask topology", **Integration, the VLSI Journal**, Vol. 2, No. 2, (1984), 85-119.

## A New Design of Dual Band Phase Shifter using MEMS Technology

B. A. Ganji, A. Razeghi

Department of Electrical and Computer Engineering, Babol University of Technology, Babol-484, IRAN

### PAPER INFO

چکیده

#### Paper history:

Received 15 November 2012

Received in revised form 23 January 2013

Accepted 18 April 2013

#### Keywords:

MEMS

Dual Band

Phase Shifter

Coplanar Waveguide

Return And Insertion Losses

این مقاله یک طراحی جدیدی از تغییردهنده‌ی فاز میکروالکترومکانیکی (MEMS) برای کاربردهای شبکه محلی بی سیم (WLAN) دو بانده ارائه می دهد. یک بیت با شیفیت فاز ثابت  $11.25^\circ$  طراحی می شود. این شیفیت فاز با سوئیچ کردن بین دو مسیر شامل سلول های واحد به تعداد متفاوت ۶ و ۱۲ در هر باند فرکانسی ایجاد می شود. یک سلول واحد از غشای طلائی معلق بر موج بر هم صفحه (CPW) ساخته می شود. غشا تحت تحریک الکتروستاتیکی می تواند به صورت عمودی حرکت داده شود و بدین ترتیب سبب تغییر باند فرکانسی کاری شود. دو حالت از سلول واحد برای سوئیچ بین دو باند فرکانسی ۲.۴GHz و ۵.۲ GHz (استاندارد IEEE 802.11 برای سیستم های WLAN دو بانده) استفاده می شود. ابتدا یک معادله ی بسته از مدل ساده ساختار بدست آورده می شود. سپس با استفاده از این معادله و شبیه ساز ADS تغییردهنده ی فاز دو بانده طراحی می شود. اعتبار مدل سازی و معادلات با استفاده از شبیه ساز ساختار فرکانس بالا (HFSS) نشان داده می شود. در فرکانس ۲.۴ GHz ماکزیمم تلفات برگشتی و جایگذاری به ترتیب برابر  $16.96\text{ dB}$  و  $-0.12$  می باشند که بهره ی شیفیت فاز  $93.75\text{ }^\circ/\text{dB}$  ( $60.22^\circ/\text{cm}$ ) به نمایش می گذارند. در فرکانس ۵.۲ GHz ماکزیمم تلفات برگشتی و جایگذاری به ترتیب برابر  $16.86\text{ dB}$  و  $-0.15$  می باشند که بهره ی شیفیت فاز  $75\text{ }^\circ/\text{dB}$  ( $60.22^\circ/\text{cm}$ ) به نمایش می گذارند. طراحی ارائه شده ی جدید تنها روش برای دستیابی به تغییر دهنده ی فاز دو بانده با استفاده از تکنولوژی MEMS می باشد که دارای تلفات و وزن پایین به همراه خطی بودن بالا نسبت به دیگر تکنولوژی هاست.

doi: 10.5829/idosi.ije.2013.26.11b.09